ChemPubSoc Europe

DOI: 10.1002/chem.201602723

CHEMISTRY A European Journal Full Paper

Ionic Liquids

Calorimetric Studies and Structural Aspects of Ionic Liquids in Designing Sorption Materials for Thermal Energy Storage

Thorge Brünig, Kristijan Krekić, Clemens Bruhn, and Rudolf Pietschnig*[a]

Abstract: The thermal properties of a series of twenty-four ionic liquids (ILs) have been determined by isothermal titration calorimetry (ITC) with the aim of simulating processes involving water sorption. For eleven water-free ILs, the molecular structures have been determined by X-ray crystallography in the solid state, which have been used to derive the molecular volumes of the ionic components of the ILs. Moreover, the structures reveal a high prevalence of hydrogen bonding in these compounds. A relationship between the molecular volumes and the experimentally determined energies of dilution could be established. The highest energies of dilution observed in this series were obtained for the acetate-based ILs, which underlines their potential as working fluids in sorption-based thermal energy storage systems.

Introduction

In the last few decades, interest in ionic liquids (ILs) has grown rapidly owing to their unique chemical and physical features.[1] In addition, they are attractive beyond their use as "designer solvents" and the tunability of their properties by variation of cation and anion allows us to tailor their versatile properties, making them useful for many fields of research and application, for example, in catalysis,[2] electrochemistry,[3] and material sciences, etc.[4] The possibility to form N-heterocyclic carbenes (NHCs) by deprotonation of 1,3-dialkylimidazolium cations makes these substances especially interesting as organocatalysts.[5] The occurrence of NHCs in ILs has been established experimentally and theoretically and suggests an increased propensity for carbene formation with strongly basic reagents or contaminants.[6] Interestingly, it was suggested that the presence of water will stabilize the ionic liquid against carbene formation and in turn also the stability of NHCs depends on the water content.[7] Moreover, the ability to absorb CO_2, involving chemisorption with formation of the corresponding NHC–CO_2 adducts either in a normal or abnormal fashion, is well established.[5b,8] Certain NHC–CO_2 adducts have been shown to equilibrate with the corresponding imidazolium hydrogen carbonates in the presence of water.[9]

With respect to the use of ILs as sorption materials for thermal energy storage, the relevant feature is the hygroscopic nature of these unique liquid electrolytes.

Solar thermal systems in combination with absorption storage systems have been shown to reduce the high energy consumption in air conditioning and furthermore open the way to seasonal energy storage concepts.[10] An important category of such systems has an open design at ambient pressure without the need for elaborate vacuum technology. In the absorber of such systems, water is absorbed from the gas phase by a highly concentrated hygroscopic electrolyte. The working fluids currently used in absorption chillers and heat pumps are LiCl or LiBr solutions, which entail problems concerning crystallization[4b], corrosion,[11] and storage capacity. Ionic liquids may be an alternative in this respect, providing tunable electrolyte properties and a higher degree of variation compared with classical inorganic salts as demonstrated in the absorption of gas (CO_2)[12] or as a desiccant owing to their hygroscopic nature.[13] In sorption storage systems, heat is released by the transition from the gas phase into the liquid phase (condensation) and in addition by hydration and dilution.[14] The IL scaffold should allow us to optimize the latter parameters, which will improve the overall performance of such a storage system. Although thermodynamically negligible, viscosity and surface tension are parameters of great practical importance for the engineering of storage devices.

The prediction of fundamental trends is performed based on molecular volumes for ionic liquids and for conventional salts.[15] These molecular parameters have also been used to explain the liquid nature of ILs at room temperature.[16] The molecular volume is closely linked to the lattice enthalpy,[17] and can be determined theoretically by DFT calculations or—if possible—experimentally from crystal structures.

In this context, we have screened a selection of ionic liquids with respect to their heats of dilution/ dissolution with the aim of determining structure–property relationships between ther-

[a] T. Brünig, K. Krekić, Dr. C. Bruhn, Prof. Dr. R. Pietschnig
Universität Kassel, Institut für Chemie und CINSaT
Heinrich-Plett-Strasse 40, 34132 Kassel (Germany)
E-mail: pietschnig@uni-kassel.de

Supporting information for this article can be found under: http://dx.doi.org/10.1002/chem.201602723.

mochemical data from calorimetric experiments and structural aspects of the ILs. For this purpose, we have examined the crystal structures of several ILs to determine the molecular volume and to assess the interaction and orientation of the anions and cations involved. The thermochemical data have been established by nanocalorimetric measurements by using isothermal titrations (ITC). With this approach, we try to improve the properties of the ILs for thermal energy storage purposes in a rational strategy and furthermore to elucidate cross-links between selected structural and thermodynamic properties of ILs.

Results and Discussion

As the corrosivity of the currently employed electrolytes towards metal-based thermal storage devices can be mainly attributed to their halide content, this aspect is relevant for the proper choice of ILs as sorption electrolytes. Even ILs with complex halide containing anions such as $[BF_4]^-$ and $[PF_6]^-$ may undergo partial hydrolysis and liberate HF.[18] Likewise, the corrosivity is largely dependent on the combination of the anion with the construction metal used.[11] In addition, other properties such as viscosity,[19] surface tension,[20] and diffusion are influenced both by the structure and the purity of ILs,[1b] where the most common contaminants are halides and/or water. Furthermore, the low melting point of $<100\,^{\circ}C$ may allow us to use neat ILs as fluids although an increased viscosity may limit the pump process within a device. Clearly, ILs with a melting point below 25 °C, so-called room-temperature ILs (RTILs), are most suitable for the envisaged energy storage applications within the human comfort zone.[21]

Because of the known properties and to minimize corrosivity, we confined ourselves to ILs with the organic anions formate, acetate, lactate, and oxalate. In addition to the improved characteristics of the subsequent application in an open sorption system, these ions are bio-compatible and seem advantageous concerning disposal after end of use. Another important point is the optimization of heat released in relation to the amount of water absorbed. This arises from the ratio of the condensation energy, which is constant at a given temperature, and the dilution energy, which will be discussed more deeply in the section below (ITC). When selecting the cations, the same considerations as for the choice of anions are applicable. Furthermore, standard variation of the cations offers modification of their desired properties. Seddon et al. described a decrease in water solubility with increasing alkyl chain length.[22] In turn, a short alkyl chain results in a higher melting point and thus a solid at room temperature. In addition to pure alkyl chains, we also considered carboxylic acid and alcohol groups attached to the 3-position in 1-methyimidazole.

Synthesis

The synthesis of the imidazolium-based ionic liquids follows established procedures, which can be divided into two steps. In the first step, 1-methylimidazole reacts with the corresponding halide (RX) in a quaternization reaction to the imidazolium salt (Scheme 1).[23,26–28] Depending on the substance, the addition of the halide is carried out in a dilute solution of 1-methylimidazole or without solvent, directly in the liquid reactant. Purification was carried out as described in the literature by recrystallization or washing with different solvents. Starting from the imidazolium halides, the anions X^1–X^3 were exchanged to X^4–X^7 in a subsequent step by using an ion exchange column according to Alcalde et al. (Scheme 2).[24]

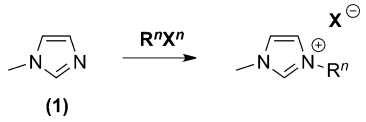

(1)

Scheme 1. Imidazolium formation through quaternization (X = Cl, Br, I).

Anion\Cation	Imidazolium						Choline
X^n\R^n	R^1: Me	R^2: Et	R^3: Pr	R^4: Iso	R^5: CH_2CH_2OH	R^6: CH_2COOH	n/a
X^1 = Cl	(11)	(16)				(8)	(2)
X^2 = Br	(10)	(4)	(5)	(6)	(7)		
X^3 = I	(3)	(17)					
X^4 = Form	(13)	(19)	(23)	(32)	(28)		(30)
X^5 = Ac	(12)	(18)	(22)	(31)	(27)		(29)
X^6 = Lac	(14)	(20)	(24)				
X^7 = NO_3	(15)	(21)					
X^8 = HCO_3			(25)	(26)			

Scheme 2. Survey of imidazolium- and choline-based ILs prepared in this investigation.

Following the same exchange procedure, choline chloride has been transformed into the corresponding formate and acetate. A survey of the ILs under investigation is summarized in Scheme 2. The completeness of the anion exchange was compared by integration of the ^1H NMR spectra between anion and cation and in addition with a silver test.[25] Furthermore, the water content was determined by Karl Fischer titration. Owing to their hygroscopic nature, all compounds were stored under a dry and inert atmosphere by using a dry box or Schlenk techniques. Thanks to the high purity of the compounds they were obtained as solids and crystal structures could be obtained for ILs **3**, **7**, **8**, **12**, **13**, **19**, **25**–**30** (see below). Apart from **8**, this is the first time structural data are available for these compounds to the best of our knowledge.[26] In addition, a crystal structure has been reported for the closely related diethylimidazolium acetate not included in our investigations.[8a] The scarcity of structural information may be attributed to the sensitivity of these solids towards trace impurities, in particular halides and water, which immediately liquefies the samples. Consequently, the solid nature of these structures further corroborates the purity of these ILs obtained by the anion exchange method.

It has been shown that certain ILs may undergo transformations to carbenes at elevated temperature, which therefore explains some of their unusual properties. Furthermore, it has been demonstrated that the gas-phase carbene formation is related to the basicity of the anion.[6] Also in our case, temperature may influence the composition of some ILs. In the case of [PMIM][Form] and [IsoMIM][Form], we observed slow transformation of the formate anion to hydrogen carbonate upon heating under vacuum below 100 °C for 24 h. The thermal decomposition of, for example, sodium formate to sodium hydrogen carbonate via sodium oxalate is well established at temperatures beyond 200 °C.[27] Transformation of formate to carbonate by an oxidant can be excluded, since the samples were exposed to argon atmosphere only, besides vacuum. In light of the recent interest in the formate–carbonate equilibrium for hydrogen storage purposes,[28] one might speculate that the special setting of the ionic liquid involving the above mentioned catalytically active carbene species may facilitate the dehydrogenative decomposition of formate. For an application as sorption media for thermal energy storage purposes this property, in turn, limits the thermal stability of formate-based ILs. The identity of the resulting hydrogen carbonates could be unambiguously confirmed by single-crystal structures for the propyl- and isopropyl imidazolium species **25** and **26**. The hydrogen carbonate-based ILs **13**, **19**, **25**, **26** show poorer solubility in polar organic solvents and also in DMSO compared with the above mentioned carboxylates and in addition they exhibit lower hygroscopic properties. Nevertheless, they need to be stored in a dry atmosphere, as well, to maintain the purity of the samples.

Isothermal titration calorimetry (ITC)

The hygroscopic properties vary widely between ILs.[29] Not only the rate of absorption, but also the reduction of the vapor pressure is an important criterion for sorbent selection for thermal storage applications. It has been shown that the anion plays a more significant role in the absorption process and, moreover, has a strong influence on the miscibility with water.[1b,30] Water solubility over a wide range is a basic requirement for use as the absorbing medium in a sorption-based thermal storage system. It has been shown that there are different aspects of interaction of water with imidazolium-based ILs as a function of dilution.[7,31]

In addition to the analysis of the IR spectra, isothermal titration calorimetry (ITC) provides a useful tool to determine the interaction between water and IL as a function of dilution. The energy released is dissipated as heat to the system, which can be monitored by ITC. Following a Born–Haber cycle, the underlying processes can be divided into the following fundamental steps:[32]

1. separation of water to free water molecules (*endothermic*);
2. evaporation of the salt into the vacuum, consuming the lattice energy (*endothermic*);
3. hydration of ions with free water molecules (*exothermic*).

The sum of these processes is substantially determined by steps 2 and 3. With large lattice energy or small hydration energy, the solution process may well be endothermic.

Dilution energies of ILs

In the context of sorbents for thermal energy storage, the contribution of the hydration energy was mostly neglected so far. The main contribution in the heat releasing sorption step is the condensation energy, which renders about $-44\ kJ\,mol^{-1}\,H_2O$.[33] Moreover, the heat of solution is usually taken into consideration for sorption processes, although the tabulated values refer to low concentrations and infinite dilution, which differs substantially from the conditions actually used in thermal energy storage applications (e.g., 44 wt% LiCl).[34] At higher concentrations, values of LiCl with about $-5.4\ kJ\,mol^{-1}\,H_2O$ and $CaCl_2$ with $-2.55\ kJ\,mol^{-1}\,H_2O$ have been reported for technically important electrolytes.[34]

As in a real sorption process only a limited concentration range is used, the heat of solution is not fully released. Therefore, we are convinced that only the heat of dilution over a certain concentration range is relevant to compare different liquid sorbents. By using ITC, we experimentally determined the energies of dilution for a series of ILs, in comparison to LiCl as a benchmark, which is currently in use in commercial devices (Figure 1). The ITC data show that the dilution energy of ILs can be quite substantial. In fact, several ILs provide substantially higher heats of dilution than LiCl. The most exothermic value was determined for [EMIM][Ac] amounting to $-14.5\ kJ\,mol^{-1}\,H_2O$, which is almost three times the value of LiCl and almost one third of the heat of condensation of water.

Changing the cation from [EMIM][Ac] to [MMIM][Ac] reduces the heat of dilution by approximately $-2.7\ kJ\,mol^{-1}$. Moreover, [MMIM][Ac] is liquid over a smaller concentration range and requires some initial water to become liquid at room temperature, making it less attractive for practical application. From the titration results, it is clear that the highest energies of dilution were found for acetate-based ILs. Thus, the heat of dilution of [EMIM][Ac] is approximately $-6.4\ kJ\,mol^{-1}\,H_2O$ larger than its formate analog and the corresponding value for [MMIM][Ac] is approximately $-3.6\ kJ\,mol^{-1}\,H_2O$ higher than its formate salt.

Also, the corresponding lactate salts, [MMIM][Lac] and [EMIM][Lac], release about $-3.6\ kJ\,mol^{-1}$ and $-5.5\ kJ\,mol^{-1}$ lower energies than the respective acetates.

Overall, the titrations indicate that for the ILs under investigation the anion largely determines the heat of dilution. Based on this, [EMIM][Ac] shows a very good compromise between the strong interaction of ions with water and, moreover, it is liquid over the entire concentration range. Furthermore, the heat of dilution obtained for a concentration range relevant for application is not only substantially higher than that of LiCl, but amounts to one third of the condensation energy of water and therefore should be quite relevant for the overall performance of sorption-based thermal energy storage devices. For direct comparison, the energy released by the sorption of one mole of liquid water into 1 kg of liquid sorbent amounts

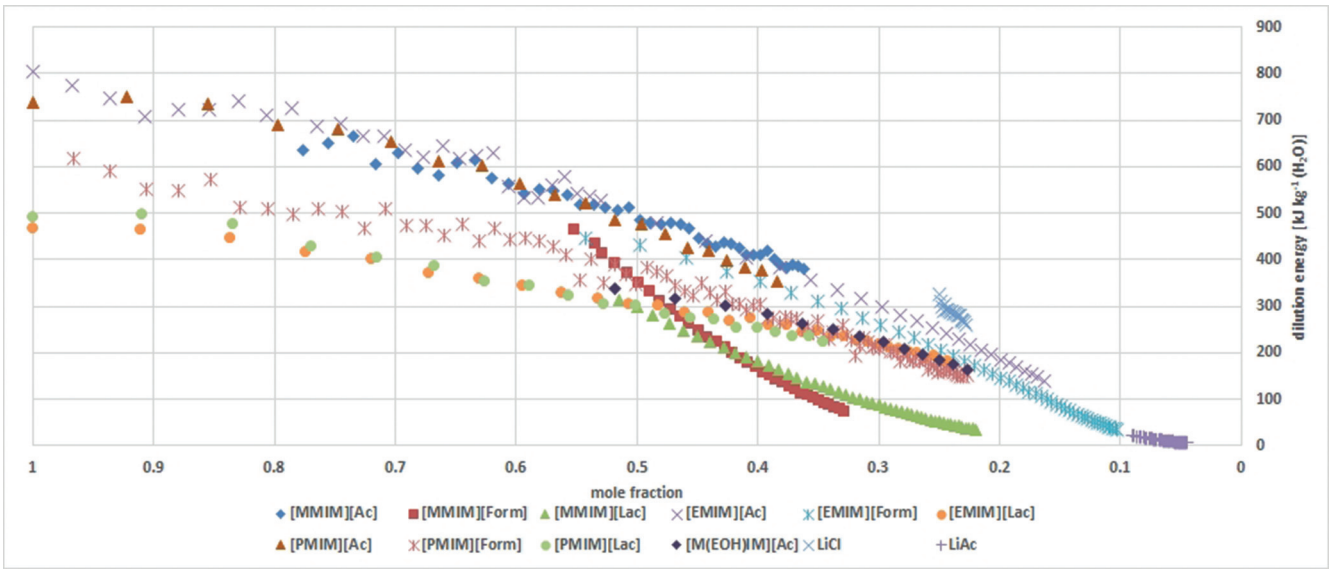

Figure 1. Plot of the heat of dilution against the mole fraction of several ILs compared with LiCl and LiAc.

to 13.2 kJ for [EMIM][Ac] compared with 6.7 kJ for LiCl solution. Related to the volume, sorption of one mole of liquid water into one liter of liquid sorbent amounts to 13.3 kJ for [EMIM][Ac] versus 7.2 kJ for LiCl solution.

Determination of molecular structures

The molecular structures of compounds **3**, **7**, **12**, **13**, **19**, **25**–**30** have been determined by single-crystal X-ray diffraction. Within the series of imidazolium structures, no large deviations of structural parameters within the cations or the respective anions are observed. Nevertheless, a medium strong hydrogen bond (O–H···H) between cation and anion is frequently observed, as exemplified by the molecular structures of choline-based **29** and **30** (Figures 2 and 3). From the solid-state data, no evidence for a zwitterionic character of the choline moiety can be derived.

Imidazolium-based ILs containing aliphatic side chains on nitrogen (**3**, **12**, **13**, and **19**, Figures 4, 6, and 7) do not show any interactions in the packing between sheets. In the molecular structures of **7**, **27**, and **28** (Figure 5 and in the Supporting Information), the ethanol side chains are turned almost perpendicular to the respective imidazolium ring. The torsion angles (C11-N11-C14-C15) are 86(3)°, 109.99(62)°, and 89.47(30)°, respectively. Several hydrogen bonds are found in these structures and these bonds influence the unique packing within the solid state of ILs (Table 1). The presence of hydrogen bonds involving the "abnormal" C–H can be observed for **12**, **13**, **25**, and **26**. Owing to the lack of structural information for ILs in general, this feature is difficult to judge, however, it is closely related to findings for abnormal hydrogen bonding in NHCs.[8b,35]

In structures **27** and **28**, very weak hydrogen bonds (C–H···O) are observed and are electrostatically stabilized. Those bonds serve as bridges between two cations over an anion and form a sheet pattern in structure **28** and a herringbone

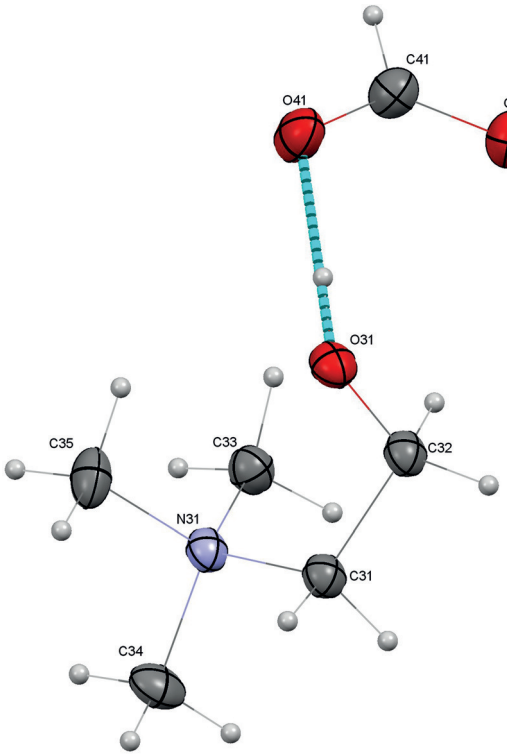

Figure 2. ORTEP plot of **30** with the corresponding hydrogen bond. One ion pair is omitted for clarity. Ellipsoids are drawn at the 30% probability level.

pattern in structure **27** (Figure 5). These patterns are connected through another hydrogen bond, O–H···O. In structures **27** and **28**, there is no evidence for zwitterionic moieties or conjugated acid of the corresponding anions.

The packing pattern of structure **12** (Figure 6) shows a wrinkled sheet motif, whereas the packing pattern of **13** (Figure 7) shows a slight bending of the planar motif, forming zigzag-like sheets. Structure **19** shows a pure planar sheet motif. Two cations are bridged by one anion through very weak hydrogen

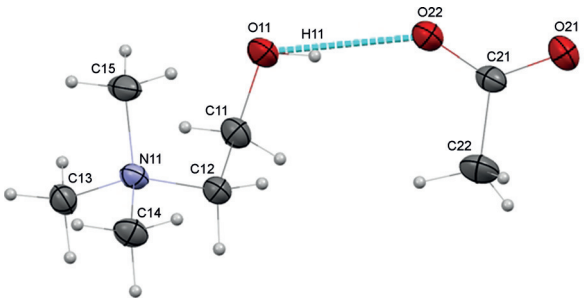

Figure 3. ORTEP plot of **29** with the corresponding hydrogen bond. Ellipsoids are drawn at the 30% probability level.

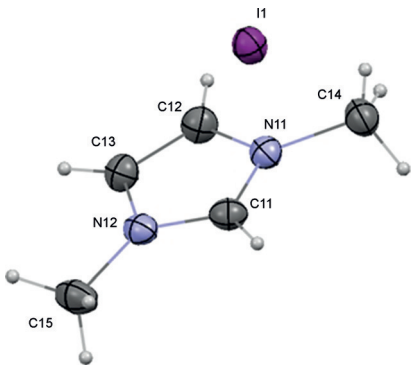

Figure 4. ORTEP plot of **3**. Ellipsoids are drawn at the 30% probability level.

bonds similar to those observed in structures **27** and **28**. As with the former imidazolium structures, evidence for a zwitterion could not be obtained.

In structures **25** and **26**, the hydrogen carbonate anion is involved in several different hydrogen bonds to the imidazolium ring as evident from a C–H···O weak hydrogen bond, which is stabilized electrostatically like in the previous structures (Figure 8). This bonding system in structure **26** leads to a sheet-like pattern of imidazolium rings, which are connected via hydrogen carbonate anions. Structure **25** shows no special packing but only hydrogen-bonded dimers of hydrogen carbonate anions. The same dimer can be observed in structure **26** (see the Supporting Information).

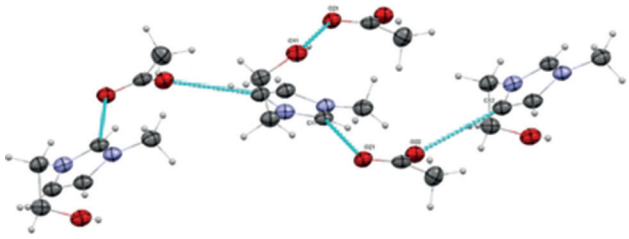

Figure 5. Packing of **27** with the corresponding hydrogen bonds. Ellipsoids are drawn at the 30% probability level.

Relationship between molecular volume and heat of dilution

The ITC measurements show that both the cation and anion influence the dissolution behavior of the ionic liquid in water. To study the dilution process in more detail, all titrations were performed at the same concentration (mole fraction of 0.5 IL/H_2O). At this concentration, the ILs are completely dissolved, and the heat released can be attributed to a progressive hydration of the ions. As already mentioned in the Introduction, the prediction of physical properties by means of a relationship to the molecular volume has been established by Krossing

Table 1. Hydrogen bonds of **27**, **28**, **12**, **13**, **19**, **26**, and **25**.

Structure	Bond	*d* (D–H) [Å]	*d* (H···A) [Å]	*d* (DH···A) [Å]	Angle (D–HH···A) [°]	Symmetry operator
27	O11–H12···O21	0.84	1.82	2.651(6)	168	$x, 1+y, z$
	C11–H11···O22	0.92(6)	2.34(6)	3.246(7)	166(5)	
	C12–H12A···O22	0.95	2.17	3.099(7)	164	$-x, -1-y, -1/2+z$
	C13–H13···O11	0.95	2.35	3.286(7)	168	$1/2+x, -y, z$
28	O11–H12···O21	0.88(4)	1.79(4)	2.654(3)	166(3)	
	C11–H11···O22	0.91(4)	2.13(4)	3.032(3)	168(4)	$-1-x, 1/2+y, -1-z$
	C12–H12A···O21	0.97(4)	2.23(3)	3.196(3)	174(3)	$-x, 1/2+y, -z$
12	C11–H11···O41	0.948(19)	2.109(19)	3.025(2)	162.1(17)	$1-x, 1-y, 1-z$
	C12–H12···O21	0.920(19)	2.274(19)	3.158(2)	161.1(17)	$-x, 1-y, 1-z$
	C31–H31···O41	0.914(19)	2.082(19)	2.986(2)	169.5(17)	
	C32–H32···O42	0.957(19)	2.208(19)	3.092(2)	153.1(15)	$1-x, -1/2+y, 3/2-z$
	C33–H33···O21	0.919(19)	2.252(19)	3.163(2)	170.7(16)	$x, y, 1+z$
13	C11–H11···O22	0.98(4)	2.01(4)	2.973(3)	170(3)	
	C32–H32···O41	0.95	2.25	3.189(3)	170	$1-x, 1-y, 1-z$
	C33–H33···O21	0.95	2.25	3.192(3)	170	$x, y, 1+z$
19	C11–H11···O21	0.97(4)	2.05(3)	3.000(4)	167(3)	$2-x, -y, 1-z$
	C13–H13···O21	0.95	2.21	3.095(4)	154	$2-x, -y, -z$
26	O22–H22···O23	0.931(17)	1.740(17)	2.6596(10)	168.9(16)	$1-x, 2-y, 1-z$
	C11–H11···O21	0.948(13)	2.095(13)	3.0212(11)	165.3(11)	
	C12–H12···O23	0.937(13)	2.296(12)	3.1726(10)	155.5(12)	$-1+x, -1+y, z$
	C13–H13···O21	0.946(14)	2.246(14)	3.1143(11)	152.2(11)	$-1+x, y, z$
25	C11–H11···O11	0.90(2)	2.34(2)	3.136(2)	147.8(19)	$-x, -y, -z$
	C13–H13···O11	1.00(2)	2.23(2)	3.122(2)	148.4(18)	$1/2-x, -1/2-y, -z$

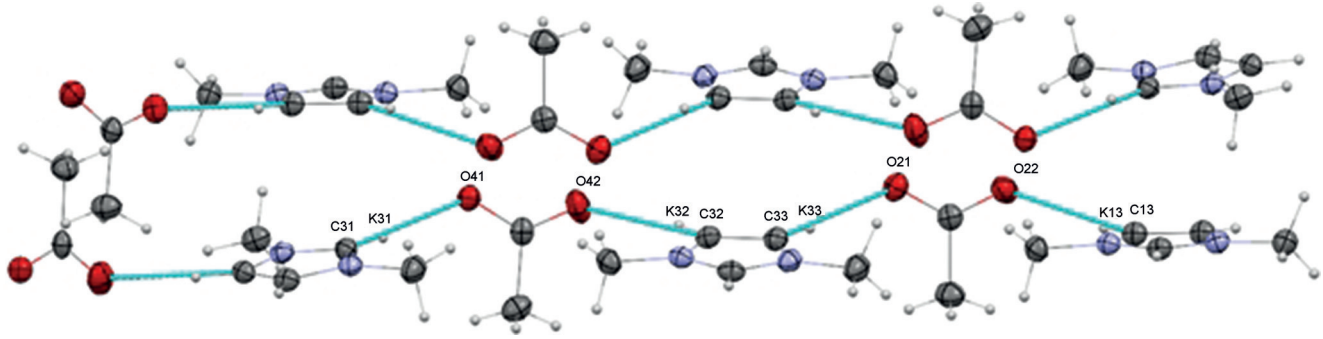

Figure 6. Packing of **12** with the corresponding hydrogen bonds. Ellipsoids are drawn at the 30% probability level.

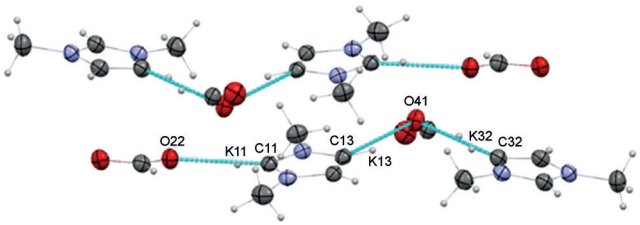

Figure 7. Packing of **13** with the corresponding hydrogen bonds. Ellipsoids are drawn at the 30% probability level.

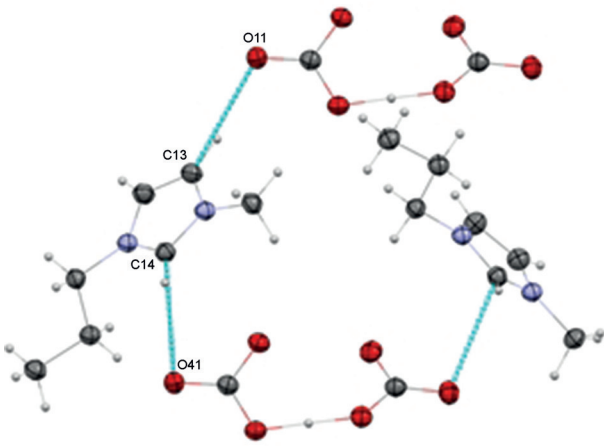

Figure 8. ORTEP plot of **25** with the corresponding hydrogen bond. Ellipsoids are drawn at the 30% probability level.

et al.[15b] The molecular volume (V_m) is defined as the sum of the individual volumes of the ions (for a binary salt of the formula AX).

$$V_m(AX) = V_{ion}(A^+) + V_{ion}(X^-) \quad (1)$$

For the calculation of the molecular volume, different methods exist. Jenkins et al.[17a] use the ionic radii of the cation (r_+) to calculate the cationic volume (V_+).

$$V_+ = \frac{4\pi r_+^3}{3} \quad (2)$$

With this value, it is now possible to get the anionic volume (V_-) by subtraction of the cell volume (V_{cell}) divided by the number of formula units with the cationic volume (method A).

$$V_- = \frac{V_{cell}}{Z} - V_+ \quad (3)$$

In this approach, however, the free volume between the ions is added to that of the anion, whereby the volume of the latter is artificially increased. Nevertheless, the molecular volume (V_m) in total remains correct by this calculation. An improved method was presented by the same authors in 2008 (method B).[36] In this case, the free volume is now distributed equally between the cation and anion. In addition to the above mentioned methods, it is possible to separate the free volume from the molecular volume by calculation of the Hirshfeld surface[37] within the unit cell of a crystal (method C).[38] Here, we use the experimental data of the substances **3**, **7**, **12**, **13**, **19**, and **25**–**30** to determine the molecular volumes. Calculation of the individual volumes for the ILs are listed in Table 2.

In particular, the evaluation according to the older method shows a large deviation from the calculation of the Hirshfeld

Table 2. The ionic volumes were calculated according to methods A–C. Values calculated with method A deviate substantially compared with those calculated by methods B and C.

Ion	V_{ion} [nm^3] (A)	V_{ion} [nm^3] (B)	V_{ion} [nm^3] (C)
[MMIM]	0.127 ± 0.015[a]	0.143 ± 0.007[b]	0.133
[EMIM]	0.156 ± 0.018[a]	0.169 ± 0.007[b]	0.144
[PMIM]	0.178 ± 0.028[a]	–	0.178
[IsoMIM]	0.173[e]	–	0.179
[M(EOH)IM]	0.157[e]	0.177[e]	0.166
[Cholin]	0.151[e]	0.170[e]	0.151
[Form]	0.064[e]	0.042[e]	0.042
[Ac]	0.049[e]	0.06[e]	0.067
[Lac]	0.101[e]	–	–
[Cl]	0.047 ± 0.013[c]	0.03 ± 0.00005[d]	0.028
[Br]	0.056 ± 0.014[c]	0.036 ± 0.00005[d]	0.037
[I]	0.072 ± 0.016[c]	0.049 ± 0.00005[d]	0.053
[NO_3]	0.064 ± 0.011[c]	0.049 ± 0.00005[d]	0.051
[HCO_3]	0.064 ± 0.003[c]	–	0.050

[a] Taken from Ref. [16]. [b] Taken from Ref. [39]. [c] Taken from Ref. [17a]. [d] Taken from Ref. [36]. [e] Calculated with method A. [f] Calculated using method B.

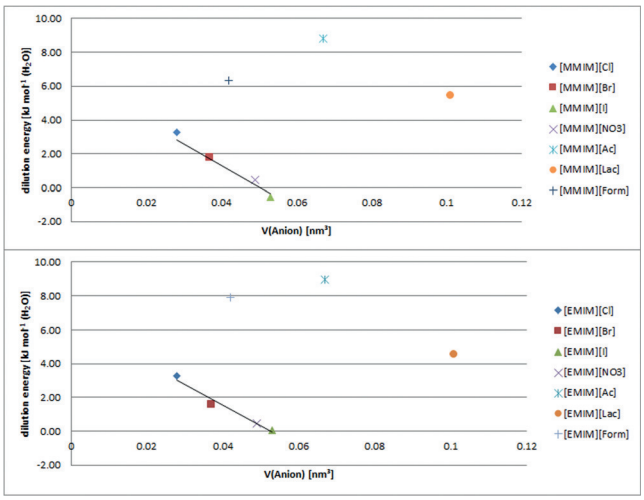

Figure 9. Plot of the dilution energy against the molecular volume of the anion (method C). Experimental measurements carried out for the MMIM salts (top) and the EMIM salts (bottom) at a 1:1 molar ratio of IL/water. For the lactate salts, no crystal structure is available and therefore the volume according to method A has been included for completeness.

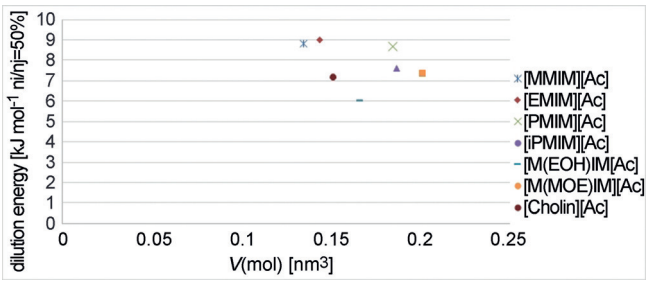

Figure 10. A comparison of the heat of dilution for different cations with the acetate anion shows that highest dilution enthalpies are achieved for alkyl imidazolium cations. Ether or alcohol functional groups lower the dilution enthalpies. The reported energy values refer to a 1:1 molar ratio of IL/water.

surfaces with an over represented size of the anions. A plot of the heats of dilution per mol against the anion size obtained by method C is shown in Figure 9.

From the graphs it is clearly visible that not only the size of the anion, but also its nature influences the heat of dilution. The decrease in the heat of dilution for a titration of ILs with inorganic anions is close to linear. With increasing size, the effective charge decreases, which also reduces the size of the hydration shell. The compounds with organic anions provide a much larger heat of dilution despite of an almost identical size. This may be explained either by a stronger interaction between water and the anions, or by a weaker interaction between the anion and cation. The anion–cation interaction is also reflected in the melting points of these ILs, which are above room temperature for the halides, nitrates, and formates, but below room temperature for the acetates and lactates. As mentioned above, the charge density at the surface of the ions is expected to be relevant for the anion–cation interaction. Furthermore, the latter may be less efficient for anisotropic anionic entities of low symmetry, which would agree with our findings. Surprising to us, the symmetry of the cation seems to be less important. Therefore, the trends of the released heats for the [MMIM] and the [EMIM] cations are almost identical. In both cases, the acetate species renders a larger heat of dilution compared with the corresponding formate, even though it has a smaller ionic radius, and thus a higher effective charge. In all exothermic titrations, no endothermic signal forms could be observed, which would suggest a separation of the cation from the anion by water. As outlined before, the anion largely determines the heat of dilution. However, cations with functional groups such as ethers or alcohols may also influence this energy (Figure 10). Moreover, strong anion–cation interaction may further limit the interaction with absorbed water as, for instance, in lithium acetate, which shows only limited solubility in water and very low dilution energies (Figure 1).

A comparison of the acetate salts of different organic cations shows energies between $-4.7\,kJ\,mol^{-1}\,H_2O$ and $-9.0\,kJ\,mol^{-1}\,H_2O$. The results show no comprehensive trend. Structural variation of the cations indicates that the energies depend on the functional groups but also on the molecular volume. The imidazolium cations with straight alkyl chains ([MMIM], [EMIM], [PMIM]) release comparable heat.

Analysis of the solution process of ILs

ITC provides the possibility to record the energy profile of the dilution or dissolution of a substance, by partial addition of water. This method does not only allow us to measure the heat energy exchange but also tracks different stages of the hydration processes on incremental addition of water in the µL range. The different hydration behavior can be related to differences in the crystal structures of the ILs under discussion.

During ITC measurements of the neat substances, compounds **7**, **12**, **13**, **27**–**30** show a transition from an initial endothermic to a subsequent exothermic process. Depending on the substance, this transition occurs after addition of only very small amounts of water.

In the case of [MMIM][Ac] **12**, the transition from endothermic to an exothermic signal occurs at a ratio of about 14:1 for IL to water, which amounts to $24.4\,kJ\,mol^{-1}\,H_2O$. This corresponds to a mole fraction of 93.28 %.

At this high concentration, it may be more meaningful to describe the mixture as a solution of water in the ionic liquid.[40] Therefore, initial processes such as breaking the crystal lattice and entropy-driven cleavage of attractive forces among water molecules in favor of water–IL interactions may result in the observed endothermic signal. With increasing amounts of water, the exothermic contribution of the solution process predominates this behavior, which could be attributed to ion hydration. The amount of heat released by this process increases up to a value of about $-12\,kJ\,mol^{-1}\,H_2O$ at a mole fraction of 73.51 % and a ratio of about 3:1 IL to H_2O. In addition, the solution process was independently tracked outside

of the calorimeter and this confirmed an initial decrease followed by a subsequent increase in sample temperature.

By changing from acetate to formate **13** with the same cation, 1,3-dimethylimidazolium, the transition from endothermic to exothermic was observed at a ratio of 2:1 IL/H_2O. The maximum exothermic quantity is released at a ratio of 3:2 IL/H_2O with an energy of $-8.1\ kJ\,mol^{-1}\,H_2O$.

A similar solution behavior in the titration analysis was found for the alcohol-substituted imidazolium salts **27** and **28**. For an endothermic–exothermic transition in the case of the acetate species, a ratio of about 16:1 IL/H_2O is required, whereas the formate species requires a ratio of 4:1 IL/H_2O for an exothermic titration signal.

For compound **29**, this transition is located in an even narrower concentration range. At a ratio of 3:1, a strong endothermic peak at about $8.2\ kJ\,mol^{-1}\,H_2O$ was measured, whereas the amount of heat increases at a ratio of 5:2 to approximately $-8.2\ kJ\,mol^{-1}\,H_2O$. Again—as for all other titrations—the maximum amount of heat released by the process could be associated with a transition from the solid to the liquid state. In contrast to the imidazolium-based ILs, the endothermic–exothermic transition of [Cholin][Form] **30** occurs at a higher ratio than that of the acetate species **29**. The calculation results in a ratio of 13:1 and a maximum endothermic signal of $12.0\ kJ\,mol^{-1}\,H_2O$. This increases to an exothermic signal of $-6.3\ kJ\,mol^{-1}\,H_2O$ at a ratio of 5:1. A survey of the ratios of IL/H_2O and the endothermic to exothermic transition is summarized in Table 3.

Table 3. The different ratios for the maximum exothermic dilution enthalpy (ΔH^{dil}_{max}) and the ratio for the transition from an endothermic to exothermic titration signal.

Ratio IL/H_2O	[**12**]	[**13**]	[**29**]	[**30**]
ΔH^{dil}_{max}	3:1	3:2	5:2	5:1
endotherm→exotherm	14:1	2:1	3:1	4:1
Ratio IL/H_2O	[**27**]	[**28**]	[**7**]	
ΔH^{dil}_{max}	4:1	2:1	1:1	
endotherm→exotherm	16:1	4:1	6:5	

Conclusion

We have determined the molecular structures of a series of ionic liquids in the solid state by X-ray diffraction. Based on these experimental structural data, the molecular volumes of the ions constituting the ILs have been derived. Furthermore, the heat flow upon addition of water of the same ILs has been determined and related to the previously obtained molecular volumes. For the more symmetric inorganic anions, such as halides and nitrate, a linear relationship between energy and dilution and molecular volume of the anion could be established. In turn, higher energies of dilution have been observed for the lower symmetric organic anions, such as acetate, formate, and lactate, which may likely be attributed to the reduced lattice energies/cation–anion interactions for the latter, leaving them more prone to interaction with water. In particular, high dilution energies have been observed for imidazolium acetates, which in the context of water sorption amount to roughly one third of the condensation energy of water itself. These results provide guidance for the design and selection of liquid electrolytes for applications such as thermal energy storage systems for improved energy management in industrial and domestic settings.

Experimental Section

All chemicals were purchased and partially purified by standard techniques, as describe in the literature. To ensure the high purity of the ionic liquids, some reactants, such as 1-methylimidazole, and the solvents were distilled and dried if necessary. The syntheses were carried out under standard inert gas conditions. The ionic exchange reactions were carried out by means of the resin Amberlyst A-26 in the OH^- form, which was purchased from Sigma–Aldrich.

The ^1H and ^{13}C NMR spectra were recorded with a MR 400 MHz Varian spectrometer (measurement frequencies: $^1H = 400$ MHz; $^{13}C = 100.5$ MHz). The chemical shifts are reported in ppm and the coupling constants in Hz. The solvents were $CDCl_3$, [D_6]DMSO, CD_2Cl_2, and D_2O. For ^1H and ^{13}C NMR measurements, the respective solvent peaks were used as the internal standard.

X-ray diffraction measurements were performed with a Stoe StadiVari with Dectris Pilatus 200 K detector or Stoe IPDS 2 with STOE image plate detector (diameter 34 cm), both using monochromatic $Mo_{K\alpha}$ radiation from a Mo Genix source with $\lambda = 0.71073$ Å. The structures were solved by using direct methods (SHELXL-2014) and refined by full-matrix least-squares techniques against F^2 (SHELXL-2014).[41] The non-hydrogen atoms were refined with anisotropic displacement parameters without any constraints. The H atoms on the imidazolium rings, located at the carbon between two nitrogen atoms, were found in the differential Fourier map and refined without any constrains. Further programs used for analysis and visualization of structural information include WinGX, Parst, and Mercury.[42] Details of the structure determinations and refinement for **3**, **7**, **12**, **13**, **19**, **25**–**30** are summarized in Table 4–6. CCDC 1483338–1483348 contain the supplementary crystallographic data for this paper. These data are provided free of charge by The Cambridge Crystallographic Data Centre.

The thermal analysis of the heat of dilution and the heat of the solution process was carried out with a TAM III from TA Instruments, equipped with a nanocalorimeter. The isothermal titration calorimetry (ITC) was carried out in 1 mL and 4 mL glass ampoules. The ITC measurements were carried out in part with solids without stirring or with the appropriate solutions in water, with stirring frequencies between 100 rpm and 200 rpm. As a stirrer, a gold propeller was used. The added amount of water and the operating time between injections were adjusted to the respective experiment. It should be noted that the statistical error of each measurement is smaller if more measurements are taken in this concentration range. The concentration given in mass percent [m%] or [$mole\,L^{-1}$] always refers to the concentration at the start of the injection of water. The greater the amount of water in relation to the presented mass, the greater the concentration range covered in the measurement. As the samples were measured and handled at isobaric conditions in ambient air with relative humidity [RH] between 30% RH and 50% RH, minimal absorption of water before the start of the experiment could not be avoided (Table 7). The

Table 4. Details of the structural determinations and refinement for **3**, **7**, **12**, and **13**.

	3	**7**	**12**	**13**
Empirical formula	$C_5H_9IN_2$	$C_6H_{11}BrN_2O$	$C_7H_{12}N_2O_2$	$C_6H_{10}N_2O_2$
Formula weight	224.04	207.08	156.19	142.16
Crystal description	Colorless plate	Colorless block	Colorless block	Colorless block
Crystal size [mm]	0.320×0.223×0.060	0.320×0.280×0.220	0.600×0.430×0.240	0.440×0.240×0.210
Crystal system, space group	orthorhombic, *Pbca*	monoclinic, $P2_1$	monoclinic, $P2_1/c$	triclinic, $P\bar{1}$
Radiation, λ [Å]	$Mo_{K\alpha}$, 0.71073	$Mo_{K\alpha}$, 0.71073	$Mo_{K\alpha}$, 0.71073	$Mo_{K\alpha}$ 0.71073
Monochromator	plane graphite	plane graphite	graded multilayer mirror	plane graphite
T [K]	173(2)	173(2)	173(2)	173(2)
Unit cell dimensions:				
a [Å]	8.8928(9)	7.3270(7)	9.8803(6)	6.5765(6)
b [Å]	17.1834(17)	7.1871(4)	16.0002(11)	8.3521(8)
c [Å]	10.5979(16)	8.5514(8)	10.3395(6)	13.8883(13)
α [°]	90.00	90.00	90.00	101.162(7)
β [°]	90.00	109.042(8)	95.177(5)	94.084(7)
γ [°]	90.00	90.00	90.00	94.507(7)
V [Å^3]	1619.4(3)	425.67(6)	1627.87(18)	743.19(12)
Z	8	2	8	4
Calculated density	1.838	1.616	1.275	1.271
F(000)	848	208	672	304
Linear absorption coefficient μ [mm^{-1}]	3.869	4.768	0.094	0.097
Absorption correction	Integration	Integration	Integration	Integration
Unit cell determination	STOE *x*-red	STOE *x*-red	STOE *x*-red	STOE *x*-red
Diffractometer	STOE IPDS 2	STOE IPDS 2	STOE StadiVari	STOE IPDS 2
Radiation source	Mo-genix	Mo-genix	Mo-genix	Mo-genix
Scan type	Omega	Omega	Omega	Omega
Θ range for data collection	1.18–25.20	2.52–25.87	1.98–28.30	1.50–25.92
Index ranges	$-10<h<9$	$-8<h<8$	$-11<h<12$	$-7<h<7$
	$-20<k<20$	$-8<k<8$	$-19<k<19$	$-9<k<8$
	$-12<l<10$	$-9<l<10$	$-7<l<12$	$-16<l<16$
Refl. collected/unique	5398/1382	2341/1521	17262/3184	5769/2587
Significant unique refl.	1174	1459	2485	2169
R(int), R(sigma)	0.0361, 0.0234	0.0427, 0.0239	0.0868, 0.0416	0.0241, 0.0226
Completeness to $\Theta=26.0°$	0.989	0.986	0.997	0.966
Refinement method	SHELXL-2014	SHELXL-2014	SHELXL-2014	SHELXL-2014
Data/parameters/restraints	1382/78/0	1521/98/0	3184/229/0	2587/191/0
Goodness-of-fit on F^2	1.068	1.705	1.051	1.073
Final R indices [$I>2\sigma(I)$]	0.0240	0.0497	0.0498	0.0710
R indices (all data)	0.0302	0.0527	0.0648	0.0784
Largest difference peak/hole [e Å^{-3}]	0.501/−0.618	1.351/−0.832	0.237/−0.171	0.363/−0.273

preparation took about 30 min. The maximum measured rate of absorption of water from the air by using ionic liquids is 2.1 mg H_2O h^{-1}, at an area of 0.95 cm^2 (corresponding to the bottom surface of the ampoule), at a temperature of 23 °C, and a relative humidity of 54%. The average of weighed mass within the measuring ampoule is 500 mg. This results in an error of the water content of about 0.2%, starting from an initial water content in the 1000 ppm range.

The determination of the water content was performed in a coulometric titration by using the device 7500 TitroLine KF trace of SI Analytics. The solid substances were dissolved in a suitable solvent, the water content of which had been previously determined.

Synthesis

1,3-Dimethylimidazolium iodide (3): The synthesis of substance **3** was performed according to Arduengo et al.[23a] ^{1}H NMR (500 MHz, [D$_6$]DMSO): $\delta=9.06$ (s, 1H), 7.69 (s, 2H), 3.85 ppm (s, 6H); ^{13}C NMR (100.5 MHz, [D$_6$]DMSO): $\delta=136.9$, 123.3, 35.7 ppm; m.p.: 85 °C.

1-Ethyl-3-methylimidazolium bromide (4): The synthesis of substance **4** was performed according to Chai et al.[23b] ^{1}H NMR (500 MHz, $CDCl_3$): $\delta=10.30$ (s, 1H), 7.57 (m, 2H), 4.36 (q, $J=7.6$ Hz, 2H), 4.06 (s, 3H), 1.55 ppm (t, $J=7.6$ Hz, 3H); ^{13}C NMR (100.5 MHz, $CDCl_3$): $\delta=136.9$, 123.5, 121.8, 45.1, 36.5, 15.6 ppm; m.p.: 72 °C.

1-Propyl-3-methylimidazolium bromide (5): The synthesis of substance **5** was performed according to Burrell et al.[43] ^{1}H NMR (500 MHz, CD_2Cl_2): $\delta=10.36$ (s, 1H), 7.51 (s, 1H), 7.46 (s, 1H), 4.27 (t, $J=6.2$ Hz, 2H), 4.06 (s, 3H), 1.94 (qt, $J=7.0$ Hz, 2H), 0.96 ppm (t, $J=7.0$ Hz, 3H); ^{13}C NMR (100.5 MHz, CD_2Cl_2): $\delta=137.8$, 123.6, 122.2, 51.6, 36.7, 23.8, 10.7 ppm.

1-Isopropyl-3-methylimidazolium bromide (6): The synthesis of substance **6** was performed according to Burrell et al.[43] ^{1}H NMR (500 MHz, [D$_6$]DMSO): $\delta=9.38$ (s, 1H), 7.95 (s, 1H), 7.77 (s, 1H), 4.65 (sept., $J=6.9$ Hz, 1H), 3.86 (s, 3H), 1.46 ppm (d, $J=6.9$ Hz, 6H); ^{13}C NMR (100.5 MHz, [D$_6$]DMSO): $\delta=135.4$, 123.6, 120.4, 52.1, 35.7, 22.4 ppm; m.p.: 79 °C.

1-Hydroxyethyl-3-methylimidazolium bromide (7): The synthesis of substance **7** was performed according to Han et al.[44] ^{1}H NMR (500 MHz, [D$_6$]DMSO): $\delta=9.12$ (s, 1H), 7.74 (s, 1H), 7.71 (s, 1H) 5.16 (t, $J=5.3$ Hz, 1H), 4.22 (t, $J=4.9$ Hz, 2H), 3.87 (s, 2H), 3.73 ppm (q, $J=5.3$ Hz, 2H); ^{13}C NMR (100.5 MHz, [D$_6$]DMSO): $\delta=136.7$, 123.2, 122.5, 59.2, 51.5, 35.6 ppm; m.p.: 90 °C.

Table 5. Details of the structure determinations and refinement for **19**, **25**–**27**.

	19	**25**	**26**	**27**
Empirical formula	$C_7H_{12}N_2O_2$	$C_8H_{14}N_2O_3$	$C_8H_{14}N_2O_3$	$C_8H_{14}N_2O_3$
Formula weight	156.19	186.21	186.21	186.21
Crystal description	colorless block	colorless plate	colorless block	colorless block
Crystal size [mm]	0.600×0.590×0.310	0.320×0.310×0.030	0.540×0.300×0.280	0.600×0.440×0.320
Crystal system, space group	monoclinic, $P2_1/n$	monoclinic, $C2/c$	triclinic, $P\bar{1}$	orthorhombic, $Pca2_1$
Radiation, λ [Å]	$Mo_{K\alpha}$, 0.71073	$Mo_{K\alpha}$, 0.71073	$Mo_{K\alpha}$, 0.71073	$Mo_{K\alpha}$, 0.71073
Monochromator	plane graphite	plane graphite	graded multilayer mirror	plane graphite
T [K]	100(2)	100(2)	100(2)	173(2)
Unit cell dimensions:				
a [Å]	6.6173(12)	11.3813(9)	7.1348(5)	13.6794(16)
b [Å]	15.835(3)	10.8536(6)	7.9218(7)	4.8778(4)
c [Å]	7.3475(11)	15.3693(13)	9.1483(8)	14.3518(13)
α [°]	90.00	90.00	92.981(7)	90.00
β [°]	94.892(13)	100.009(6)	108.922(6)	90.00
γ [°]	90.00	90.00	101.902(6)	90.00
Volume [Å^3]	767.1(2)	1869.6(2)	474.64(7)	957.63(16)
Z	4	8	2	4
Calculated density	1.352	1.323	1.303	1.292
F(000)	336	800	200	400
Linear absorption coefficient μ [mm^{-1}]	0.100	0.102	0.100	0.099
Absorption correction	none	integration	integration	none
Unit cell determination	STOE *x*-red	STOE *x*-red	STOE *x*-red	STOE *x*-red
Diffractometer	STOE IPDS 2	STOE IPDS 2	STOE StadiVari	STOE IPDS 2
Radiation source	Mo-genix	Mo-genix	Mo-genix	Mo-genix
Scan type	omega	omega	omega	omega
Θ range for data collection	1.29–25.86	2.61–26.17	2.37–31.91	2.06–25.84
Index ranges	$-7<h<7$ $-18<k<16$ $-6<l<8$	$-13<h<13$ $-12<k<11$ $-17<l<18$	$-10<h<9$ $-10<k<11$ $-12<l<12$	$-14<h<16$ $-5<k<5$ $-17<l<17$
Refl. collected/unique	2745/1339	4197/1651	10289/2653	4095/1679
Significant unique refl.	1068	1436	2395	1491
R(int), R(sigma)	0.0471, 0.0359	0.0479, 0.0383	0.0238, 0.0126	0.1606, 0.0869
Completeness to $\Theta=26.0°$	0.990	0.995	1.000	0.971
Refinement method	SHELXL-2014	SHELXL-2014	SHELXL-2014	SHELXL-2014
Data/parameters/restraints	1339/106/0	1651/138/1	2653/137/0	1679/124/2
Goodness-of-fit on F^2	1.139	1.036	1.041	1.061
Final R indices [$I>2\sigma(I)$]	0.0703	0.0460	0.0306	0.0786
R indices (all data)	0.0874	0.0519	0.0342	0.0838
Largest difference peak/hole [e Å^{-3}]	0.287/−0.354	0.219/−0.209	0.329/−0.191	0.212/−0.380

1-Carboxymethyl-3-methylimidazolium chloride (9): The synthesis of substance **9** was performed according to Song et al.[45] ^{1}H NMR (500 MHz, D_2O): $\delta=8.79$ (s, 1H), 7.49 (m, 2H), 5.07 (s, 2H), 3.94 ppm (s,3H); ^{13}C NMR (100.5 MHz, [D_6]DMSO): $\delta=170.0$, 137.2, 123.4, 49.9, 35.8 ppm; m.p.: 187 °C.

The halide anions of the imidazolium (**3**–**7**) and choline (**2**) cations were exchanged in a subsequent step by using an ion exchange column according to Alcalde et al.[24] The completeness of the anion exchange was compared by using the integration of the ^{1}H NMR spectra between the anion and cation and in addition with a silver test.[25] Furthermore, the water content was determined by Karl Fischer titration. Owing to their hygroscopic nature, all compounds were stored under a dry atmosphere by using a dry box or Schlenk techniques after drying. Drying was performed by heating the corresponding IL in a Schlenk flask at 65 °C (water bath) under vacuum (10^{-3} mbar) for one day.

1,3-Dimethylimidazolium bromide (10): ^{1}H NMR (500 MHz, CD_2Cl_2): $\delta=10.27$ (s, 1H), 7.43 (s, 2H), 4.05 ppm (s, 6H); ^{13}C NMR (100.5 MHz, $CDCl_3$): $\delta=137.9$, 123.4, 36.7 ppm.

1,3-Dimethylimidazolium chloride (11): ^{1}H NMR (500 MHz, $CDCl_3$): $\delta=9.82$ (s, 1H), 7.44 (s, 2H), 3.76 ppm (s, 6H); ^{13}C NMR (100.5 MHz, $CDCl_3$): $\delta=138.2$, 123.7, 37.1 ppm.

1,3-Dimethylimidazolium acetate (12): ^{1}H NMR (500 MHz, CD_2Cl_2): $\delta=11.24$ (s, 1H), 7.40 (s, 2H), 3.96 (s, 6H), 1.77 ppm (s, 3H); ^{13}C NMR (100.5 MHz, CD_2Cl_2): $\delta=175.5$, 140.0, 122.1, 35.0, 24.6 ppm; m.p.: 38 °C.

1,3-Dimethylimidazolium formate (13): ^{1}H NMR (500 MHz, CD_2Cl_2): $\delta=10.67$ (s, 1H), 8.74 (s, 1H), 7.48 (m, 2H), 3.95 ppm (s, 3H); ^{13}C NMR (100.5 MHz, CD_2Cl_2): $\delta=167.5$, 139.7, 123.2, 36.0 ppm; m.p.: 50 °C.

1,3-Dimethylimidazolium lactate (14): ^{1}H NMR (500 MHz, CD_2Cl_2): $\delta=9.95$ (s, 1H), 7.41 (m, 2H), 4.01 (s, 3H), 3.79 (q, $J=6.7$ ^{13}C NMR (100.5 MHz, CD_2Cl_2): $\delta=180.4$, 141.2, 123.2, 68.4, 36.7, 21.9 ppm.

1,3-Dimethylimidazolium nitrate (15): ^{1}H NMR (500 MHz, CD_2Cl_2): $\delta=9.71$ (s, 1H), 7.51 (m, 2H), 3.97 ppm (s, 6H); ^{13}C NMR (100.5 MHz, CD_2Cl_2): $\delta=139.8$, 125.4, 38.3 ppm.

1-Ethyl-3-methylimidazolium chloride (16): ^{1}H NMR (500 MHz, CD_2Cl_2): $\delta=10.49$ (s, 1H), 7.49 (m, 2H), 4.36 (q, $J=7.4$ Hz, 2H), 4.05 (s, 3H), 1.55 ppm (t, $J=7.4$ Hz, 3H); ^{13}C NMR (100.5 MHz, CD_2Cl_2): $\delta=136.1$, 122.8, 121.1, 45.1, 36.3, 15.9 ppm.

Table 6. Details of the structure determinations and refinement for **28**–**30**.

	28	**29**	**30**
Empirical formula	$C_7H_{12}N_2O_3$	$C_7H_{17}NO_3$	$C_6H_{15}NO_3$
Formula weight	172.19	163.21	149.19
Crystal description	colorless block	colorless plate	colorless block
Crystal size [mm]	0.410×0.260×0.230	0.510×0.350×0.040	0.370×0.250×0.160
Crystal system, space group	monoclinic, $P2_1$	monoclinic, $P2_1$	monoclinic, $P2_1/c$
Radiation, λ [Å]	$Mo_{K\alpha}$, 0.71073	$Mo_{K\alpha}$, 0.71073	$Mo_{K\alpha}$, 0.71073
Monochromator	plane graphite	plane graphite	graded multilayer mirror
T [K]	100(2)	100(2)	100(2)
Unit cell dimensions:			
a [Å]	7.1391(10)	7.6817(7)	13.7853(7)
b [Å]	7.0065(6)	7.1487(6)	10.0727(3)
c [Å]	9.2618(12)	8.4593(7)	11.5445(6)
α [°]	90.00	90.00	90.00
β [°]	111.787(10)	102.581(7)	90.480(4)
γ [°]	90.00	90.00	90.00
V [Å^3]	430.18(9)	453.38(7)	1602.96(13)
Z	2	2	8
Calculated density	1.329	1.196	1.236
F(000)	184	180	656
Linear absorption coefficient μ [mm^{-1}]	0.104	0.092	0.098
Absorption correction	integration	integration	integration
Unit cell determination	STOE *x*-red	STOE *x*-red	STOE *x*-red
Diffractometer	STOE IPDS 2	STOE IPDS 2	STOE StadiVari
Radiation source	Mo-genix	Mo-genix	Mo-genix
Scan type	omega	omega	omega
Θ range for data collection	2.37–25.89	2.47–25.84	2.31–25.86
Index ranges	$-8<h<8$	$-9<h<9$	$-14<h<16$
	$-8<k<8$	$-8<k<8$	$-11<k<12$
	$-11<l<11$	$-10<l<8$	$-13<l<13$
Refl. collected/unique	3414/1492	3306/1589	12312/2909
Significant unique refl.	1450	1480	2429
R(int), R(sigma)	0.0355, 0.0227	0.0844, 0.0548	0.0724, 0.0407
Completeness to $\Theta=26.0°$	0.986	0.966	0.998
Refinement method	SHELXL-2014	SHELXL-2014	SHELXL-2014
Data/parameters/restraints	1492/123/2	1589/107/1	2909/193/0
Goodness-of-fit on F^2	1.060	1.099	1.055
Final R indices [$I>2\sigma(I)$]	0.0384	0.0514	0.0442
R indices (all data)	0.0391	0.0547	0.0519
Largest difference peak/hole [e Å^{-3}]	0.127/−0.154	0.205/−0.211	0.218/−0.248

Table 7. Water content of the prepared ILs.

Number	Substance	H_2O [ppm]
3	[MMIM][I]	400
7	[(EOH)MIM][Br]	268
12	[MMIM][Ac]	2108
13	[MMIM][Form]	2385
14	[[MMIM][Lac]	1907
18	[EMIM][Ac]	1498
19	[EMIM][Form]	1255
20	[EMIM][Lac]	1144
22	[PMIM][Ac]	2408
23	[PMIM][Form]	2056
24	[PMIM][Lac]	1290
27	[(EOH)MIM][Ac]	985
28	[(EOH)MIM][Form]	1203
29	[Cholin][Ac]	870
30	[Cholin][Form]	978

1-Ethyl-3-methylimidazolium iodide (17): ^{1}H NMR (500 MHz, CD_2Cl_2): $\delta=10.15$ (s, 1H), 7.40 (m, 1H), 7.38 (m, 1H), 4.36 (q, $J=7.2$ Hz, 2H), 4.06 (s, 3H), 1.59 ppm (t, $J=7.2$ Hz, 3H); ^{13}C NMR (100.5 MHz, CD_2Cl_2): $\delta=136.8$, 123.6, 121.9, 45.1, 36.6, 15.6 ppm.**1-Ethyl-3-methylimidazolium acetate (18)**: ^{1}H NMR (500 MHz, CD_2Cl_2): $\delta=11.23$ (s, 1H), 7.35 (m, 2H), 4.30 (q, $J=7.4$ Hz, 2H), 3.99 (s, 3H), 1.79 (s, 3H), 1.50 ppm (t, $J=7.4$, 3H); ^{13}C NMR (100.5 MHz, CD_2Cl_2): $\delta=176.5$, 139.5, 123.0, 121.2, 44.9, 36.0, 25.1, 15.3 ppm.

1-Ethyl-3-methylimidazolium formate (19): ^{1}H NMR (500 MHz, CD_2Cl_2): $\delta=10.49$ (s, 1H), 8.69 (s, 1H), 7.59 (s, 1H), 7.57 (s, 1H), 4.24 (q, $J=7.43$, 2H), 3.92 (s, 3H), 1.42 ppm (t, $J=6.46$, 2H); ^{13}C NMR (100.5 MHz, CD_2Cl_2): $\delta=167.7$, 139.6, 122.7, 120.9, 45.0, 36.1, 15.2 ppm; m.p.: 36 °C.

1-Ethyl-3-methylimidazolium lactate (20): ^{1}H NMR (500 MHz, CD_2Cl_2): $\delta=10.51$ (s, 1H), 7.39 (m, 2H), 4.30 (q, $J=7.4$ Hz, 2H), 4.00 (s, 3H), 3.77 (q, $J=6.8$ Hz, 1H), 1.52 (t, $J=7.4$ Hz, 3H), 1.21 ppm (d, $J=6.8$ Hz, 3H); ^{13}C NMR (100.5 MHz, CD_2Cl_2): $\delta=179.6$, 138.5, 123.2, 121.4, 67.9, 45.0, 36.1, 21.4, 15.3 ppm.

1-Ethyl-3-methylimidazolium nitrate (21): ^{1}H NMR (500 MHz, CD_2Cl_2): $\delta=9.93$ (s, 1H), 7.37 (m, 1H), 7.36 (m, 1H), 4.30 (q, $J=7.4$ Hz, 2H), 3.99 (s, 3H), 1.55 ppm (t, $J=7.4$ Hz, 3H); ^{13}C NMR (100.5 MHz, CD_2Cl_2): $\delta=137.7$, 123.3, 121.6, 45.3, 36.3, 15.2 ppm.

1-Propyl-3-methylimidazolium acetate (22): ^{1}H NMR (500 MHz, CD_2Cl_2): $\delta=11.14$ (s, 1H), 7.41 (m, 1H), 7.36 (m, 1H), 4.21 (t, $J=7.4$ Hz, 2H), 4.00 (s, 3H), 1.88 (qt, $J=7.4$ Hz, 2H), 1.78 (s, 3H),

0.92 ppm (t, $J=7.4$ Hz, 3H); ^{13}C NMR (100.5 MHz, CD_2Cl_2): $\delta=176.8$, 140.7, 123.5, 122.0, 51.6, 36.5, 25.8, 24.0, 10.9 ppm.

1-Propyl-3-methylimidazolium formate (23): ^{1}H NMR (500 MHz, [D_6]DMSO): $\delta=9.50$ (s, 1H), 8.58 (s, 1H), 7.81 (m, 1H), 7.75 (m, 1H), 4.14 (t, $J=6.7$ Hz, 2H), 3.86 (s, 3H), 1.79 (qt, 2H), 0.84 (t, 3H); ^{13}C NMR (100.5 MHz, D_2O): $\delta=170.8$, 135.7, 123.3, 122.0, 50.9, 35.4, 22.7, 9.7 ppm.

1-Propyl-3-methylimidazolium lactate (24): ^{1}H NMR (500 MHz, CD_2Cl_2): $\delta=10.86$ (s, 1H), 7.29 (s, 1H), 7.26 (s, 1H), 4.21 (t, $J=7.2$ Hz, 2H), 4.01 (s, 3H), 3.79 (q, $J=6.7$ Hz, 1H), 1.90 (qt, $J=7.0$ Hz, 2H), 1.23 (d, $J=6.7$ Hz, 3H), 0.95 ppm (t, $J=7.4$ Hz, 3H); ^{13}C NMR (100.5 MHz, CD_2Cl_2): $\delta=180.0$, 140.1, 123.2, 121.8, 68.3, 51.6, 36.5, 23.9, 21.8, 10.8 ppm.

1-Propyl-3-methylimidazolium hydrogen carbonate (25): ^{1}H NMR (500 MHz, D_2O): $\delta=8.39$ (s, 1H), 7.42 (m, 1H), 7.38 (m, 1H), 4.10 (t, $J=7.0$ Hz, 2H), 3.84 (s, 3H), 1.83 (qt, $J=7.0$ Hz, 2H), 0.85 ppm (t, $J=7.2$ Hz, 3H); ^{13}C NMR (100.5 MHz, D_2O): $\delta=173.3$, 162.8, 125.8, 124.6, 53.5, 38.0, 25.3, 12.2 ppm.

1-Isopropyl-3-methylimidazolium hydrogen carbonate (26): ^{1}H NMR (500 MHz, D_2O): $\delta=8.40$ (s, 1H), 7.49 (m, 1H), 7.37 (m, 1H), 4.57 (sept., $J=6.7$ Hz, 1H), 3.83 (s, 3H), 1.49 ppm (d, $J=6.7$ Hz, 6H); ^{13}C NMR (100.5 MHz, D_2O): $\delta=160.2$, 134.2, 123.2, 120.1, 52.8, 35.4, 21.8 ppm.

1-Hydroxyethyl-3-methylimidazolium acetate (27): ^{1}H NMR (500 MHz, CD_2Cl_2): $\delta=10.30$ (s, 1H), 7.49 (s, 1H), 7.35 (s, 1H), 4.32, (t, $J=5.1$ Hz, 2H), 3.91 (s, 3H), 3.83 (t, $J=4.9$ Hz, 2H), 1.78 ppm (s, 3H); ^{13}C NMR (100.5 MHz, CD_2Cl_2): $\delta=177.3$, 139.7, 123.1, 123.0, 59.9, 52.8, 36.5, 25.4 ppm; m.p.: 57 °C.

1-Hydroxyethyl-3-methylimidazolium formate (28): ^{1}H NMR (500 MHz, [D_6]DMSO): $\delta=9.35$ (s, 1H), 8.51 (s, 1H), 7.76 (s, 1H), 7.70 (s, 1H), 6.56 (m, 1H), 4.23 (t, $J=4.9$ Hz, 2H), 3.85 (s, 3H), 3.70 ppm (t, $J=4.9$ Hz, 2H); ^{13}C NMR (100.5 MHz, [D_6]DMSO): $\delta=165.6$, 137.2, 123.3, 122.8, 59.3, 51.7, 35.7 ppm; m.p.: 50 °C.

2-Hydroxyethyl-trimethylammonium acetate (29): ^{1}H NMR (500 MHz, [D_6]DMSO): $\delta=3.82$ (m, 2H), 3.43 (t, $J=4.5$ Hz, 2H), 3.13 (s, 9H), 1.59 ppm (s, 3H); ^{13}C NMR (100.5 MHz, CD_2Cl_2): $\delta=173.7$, 67.2, 54.8, 52.9, 25.7 ppm; m.p.: 75 °C.

2-Hydroxyethyl-trimethylammonium formate (30): ^{1}H NMR (500 MHz, [D_6]DMSO): $\delta=8.53$ (s, 1H), 3.83 (m, 2H), 3.43 (t, $J=5.28$ Hz, 2H), 3.14 ppm (s, 9H); ^{13}C NMR (100.5 MHz, [D_6]DMSO): $\delta=165.7$, 67.1, 54.8, 53.0 ppm; m.p.: 40 °C.

1-Isopropyl-3-methylimidazolium acetate (31): ^{1}H NMR (500 MHz, CD_2Cl_2): $\delta=11.38$ (s, 1H), 7.31 (s, 1H), 7.29 (m, 1H), 4.76 (sept., $J=6.7$ Hz, 1H), 4.02 (s, 3H), 1.80 (s, 3H), 1.55 ppm (d, $J=6.7$ Hz, 6H); ^{13}C NMR (100.5 MHz, CD_2Cl_2): $\delta=176.7$, 140.0, 123.1, 119.4, 53.3, 36.3, 25.7, 23.1 ppm.

1-Isopropyl-3-methylimidazolium formate (32): ^{1}H NMR (500 MHz, CD_2Cl_2): $\delta=9.59$ (s, 1H), 8.59 (s, 1H), 7.92 (m, 1H), 7.76 (m, 1H), 4.64 (sept., $J=6.7$ Hz, 1H), 3.86 (s, 3H), 1.47 ppm (d, $J=6.7$ Hz, 6H); ^{13}C NMR (100.5 MHz, $CDCl_3$): $\delta=168.4$, 137.5, 123.4, 119.6, 53.0, 36.2, 23.0 ppm.

Acknowledgements

We thank Astrid Pilz for her numerous efforts in mounting the sensitive and deliquescent crystals on the diffractometer. Financial support by the BMBF project OpenSorp (T.B.) and the EU ITN SHINE (K.K.) is gratefully acknowledged. Moreover, we are grateful to Prof. Dr. Ulrike Jordan for helpful discussions.

Keywords: ionic liquids · isothermal titration calorimetry · molecular volume · water sorption · X-ray diffraction

[1] a) N. V. Plechkova, K. R. Seddon, *Chem. Soc. Rev.* **2008**, *37*, 123 – 150; b) K. R. Seddon, A. Stark, M.-J. Torres, *Pure Appl. Chem.* **2000**, *72*, 2275 – 2287; c) T. Welton, *Chem. Rev.* **1999**, *99*, 2071 – 2084.

[2] a) P. Wasserscheid, W. Keim, *Angew. Chem. Int. Ed.* **2000**, *39*, 3772 – 3789; *Angew. Chem.* **2000**, *112*, 3926 – 3945; b) S. Peleteiro, S. Rivas, J. L. Alonso, V. Santos, J. C. Parajó, *Bioresour. Technol.* **2016**, *202*, 181 – 191; c) H.-P. Steinrück, P. Wasserscheid, *Catal. Lett.* **2015**, *145*, 380 – 397.

[3] a) B. M. Quinn, Z. Ding, R. Moulton, A. J. Bard, *Langmuir* **2002**, *18*, 1734 – 1742; b) M. Galiński, A. Lewandowski, I. Stępniak, *Electrochim. Acta* **2006**, *51*, 5567 – 5580; c) J. S. Wilkes, J. A. Levisky, R. A. Wilson, C. L. Hussey, *Inorg. Chem.* **1982**, *21*, 1263 – 1264; d) R. Jindal, A. Sablok, *Curr. Green Chem.* **2015**, *2*, 135 – 155; e) M. Armand, F. Endres, D. R. MacFarlane, H. Ohno, B. Scrosati, *Nat. Mater.* **2009**, *8*, 621 – 629.

[4] a) Y. Chen, Y. Cao, T. Mu, *Chem. Eng. Technol.* **2014**, *37*, 527 – 534; b) P. Wasserscheid, M. Seiler, *ChemSusChem* **2011**, *4*, 459 – 463; c) G. Gebresilassie Eshetu, M. Armand, B. Scrosati, S. Passerini, *Angew. Chem. Int. Ed.* **2014**, *53*, 13342 – 13359; *Angew. Chem.* **2014**, *126*, 13558 – 13576; d) S. Herrmann, M. Kostrzewa, A. Wierschem, C. Streb, *Angew. Chem. Int. Ed.* **2014**, *53*, 13596 – 13599; *Angew. Chem.* **2014**, *126*, 13814 – 13817; e) R. P. Swatloski, S. K. Spear, J. D. Holbrey, R. D. Rogers, *J. Am. Chem. Soc.* **2002**, *124*, 4974 – 4975; f) J. S. Wilkes, *Green Chem.* **2002**, *4*, 73 – 80.

[5] a) O. Hollóczki, L. Nyulászi, *Org. Biomol. Chem.* **2011**, *9*, 2634 – 2640; b) O. Hollóczki, L. Nyulászi in *Carbenes from Ionic Liquids*, (Ed.: B. Kirchner), Springer, Berlin, **2014**, pp. 1 – 24.

[6] O. Holloczki, D. Gerhard, K. Massone, L. Szarvas, B. Nemeth, T. Veszpremi, L. Nyulászi, *New J. Chem.* **2010**, *34*, 3004 – 3009.

[7] a) M. Brehm, H. Weber, A. S. Pensado, A. Stark, B. Kirchner, *Phys. Chem. Chem. Phys.* **2012**, *14*, 5030 – 5044; b) O. Hollóczki, P. Terleczky, D. Szieberth, G. Mourgas, D. Gudat, L. Nyulászi, *J. Am. Chem. Soc.* **2011**, *133*, 780 – 789.

[8] a) G. Gurau, H. Rodríguez, S. P. Kelley, P. Janiczek, R. S. Kalb, R. D. Rogers, *Angew. Chem. Int. Ed.* **2011**, *50*, 12024 – 12026; *Angew. Chem.* **2011**, *123*, 12230 – 12232; b) Z. Kelemen, B. Péter-Szabó, E. Székely, O. Hollóczki, D. S. Firaha, B. Kirchner, J. Nagy, L. Nyulászi, *Chem. Eur. J.* **2014**, *20*, 13002 – 13008.

[9] a) M. Fèvre, J. Pinaud, A. Leteneur, Y. Gnanou, J. Vignolle, D. Taton, K. Miqueu, J.-M. Sotiropoulos, *J. Am. Chem. Soc.* **2012**, *134*, 6776 – 6784; b) M. Fèvre, P. Coupillaud, K. Miqueu, J.-M. Sotiropoulos, J. Vignolle, D. Taton, *J. Org. Chem.* **2012**, *77*, 10135 – 10144.

[10] a) C. Janiak, K. Henninger Stefan, *Nachr. Chem.* **2013**, *61*, 520 – 523; b) G. Grossman, *Sol. Energy* **2002**, *72*, 53 – 62; c) S. K. Henninger, F. Jeremias, H. Kummer, C. Janiak, *Eur. J. Inorg. Chem.* **2012**, 2625 – 2634.

[11] M. Uerdingen, C. Treber, M. Balser, G. Schmitt, C. Werner, *Green Chem.* **2005**, *7*, 321 – 325.

[12] a) E. D. Bates, R. D. Mayton, I. Ntai, J. H. Davis, *J. Am. Chem. Soc.* **2002**, *124*, 926 – 927; b) M. Ramdin, T. W. Loos, T. J. H. Vlugt, *Ind. Eng. Chem. Res.* **2012**, *51*, 8149 – 8177.

[13] a) Y. Chen, X. Sun, C. Yan, Y. Cao, T. Mu, *J. Phys. Chem. B* **2014**, *118*, 11523 – 11536; b) T. Köddermann, C. Wertz, A. Heintz, R. Ludwig, *Angew. Chem. Int. Ed.* **2006**, *45*, 3697 – 3702; *Angew. Chem.* **2006**, *118*, 3780 – 3785.

[14] J. Albers, A. Kühn, S. Petersen, F. Ziegler, *Chem. Ing. Tech.* **2011**, *83*, 1853 – 1863.

[15] a) J. M. Slattery, C. Daguenet, P. J. Dyson, T. J. S. Schubert, I. Krossing, *Angew. Chem. Int. Ed.* **2007**, *46*, 5384 – 5388; *Angew. Chem.* **2007**, *119*, 5480 – 5484; b) W. Beichel, U. P. Preiss, S. P. Verevkin, T. Koslowski, I. Krossing, *J. Mol. Liq.* **2014**, *192*, 3 – 8.

[16] I. Krossing, J. M. Slattery, C. Daguenet, P. J. Dyson, A. Oleinikova, H. Weingärtner, *J. Am. Chem. Soc.* **2006**, *128*, 13427 – 13434.

[17] a) H. D. B. Jenkins, H. K. Roobottom, J. Passmore, L. Glasser, *Inorg. Chem.* **1999**, *38*, 3609 – 3620; b) L. Glasser, H. D. B. Jenkins, *J. Chem. Eng. Data* **2011**, *56*, 874 – 880.

[18] a) M. G. Freire, C. M. S. S. Neves, I. M. Marrucho, J. A. P. Coutinho, A. M. Fernandes, *J. Phys. Chem. A* **2010**, *114*, 3744 – 3749; b) R. P. Swatloski, J. D. Holbrey, R. D. Rogers, *Green Chem.* **2003**, *5*, 361 – 363.

[19] K. R. Seddon, A. Stark, M.-J. Torres in *Viscosity and Density of 1-Alkyl-3-methylimidazolium Ionic Liquids, Vol. 819* (Eds.: M. A. Abraham, L. Moens), American Chemical Society, Washington, DC, **2002**, pp. 34 – 49.
[20] M. Tariq, M. G. Freire, B. Saramago, J. A. P. Coutinho, J. N. C. Lopes, L. P. N. Rebelo, *Chem. Soc. Rev.* **2012**, *41*, 829 – 868.
[21] P. L. Kramer, C. H. Giammanco, M. D. Fayer, *J. Chem. Phys.* **2015**, *142*, 212408.
[22] J. G. Huddleston, A. E. Visser, W. M. Reichert, H. D. Willauer, G. A. Broker, R. D. Rogers, *Green Chem.* **2001**, *3*, 156 – 164.
[23] a) E. M. B. Brian, L. Benac, A. J. Arduengo III, *Org. Synth.* **1986**, *64*, 92; b) S. Jana, A. Parthiban, C. L. L. Chai, *Chem. Commun.* **2010**, *46*, 1488 – 1490; c) Z. Fei, W. H. Ang, D. Zhao, R. Scopelliti, E. E. Zvereva, S. A. Katsyuba, P. J. Dyson, *J. Phys. Chem. B* **2007**, *111*, 10095 – 10108; d) F. F. D. Oliveira, M. R. dos Santos, P. M. Lalli, E. M. Schmidt, P. Bakuzis, A. A. M. Lapis, A. L. Monteiro, M. N. Eberlin, B. A. D. Neto, *J. Org. Chem.* **2011**, *76*, 10140 – 10147.
[24] E. Alcalde, I. Dinarès, A. Ibáñez, N. Mesquida, *Molecules* **2012**, *17*, 4007 – 4027.
[25] A. R. Toral, A. P. de los Ríos, F. J. Hernández, M. H. A. Janssen, R. Schoevaart, F. van Rantwijk, R. A. Sheldon, *Enzyme Microb. Technol.* **2007**, *40*, 1095 – 1099.
[26] X.-P. Xuan, L.-L. Chang, H. Zhang, N. Wang, Y. Zhao, *CrystEngComm* **2014**, *16*, 3040 – 3046.
[27] a) T. Yoshimori, Y. Asano, Y. Toriumi, T. Shiota, *Talanta* **1978**, *25*, 603 – 605; b) T. Meisel, Z. Halmos, K. Seybold, E. Pungor, *J. Therm. Anal.* **1975**, *7*, 73 – 80.
[28] G. Papp, J. Csorba, G. Laurenczy, F. Joó, *Angew. Chem. Int. Ed.* **2011**, *50*, 10433 – 10435; *Angew. Chem.* **2011**, *123*, 10617 – 10619.
[29] F. Di Francesco, N. Calisi, M. Creatini, B. Melai, P. Salvo, C. Chiappe, *Green Chem.* **2011**, *13*, 1712 – 1717.
[30] M. G. Freire, L. M. N. B. F. Santos, A. M. Fernandes, J. A. P. Coutinho, I. M. Marrucho, *Properties and Phase Equilibria for Product and Process Design 11th International Conference on Properties and Phase Equilibria for Product and Process Design* **2007**, pp. 449 – 454.
[31] a) Y. Chen, S. Li, Z. Xue, M. Hao, T. Mu, *J. Mol. Struct.* **2015**, *1079*, 120 – 129; b) T. Takamuku, Y. Kyoshoin, T. Shimomura, S. Kittaka, T. Yamaguchi, *J. Phys. Chem. B* **2009**, *113*, 10817 – 10824; c) L. Cammarata, S. G. Kazarian, P. A. Salter, T. Welton, *Phys. Chem. Chem. Phys.* **2001**, *3*, 5192 – 5200; d) S. Cuadrado-Prado, M. Domínguez-Pérez, E. Rilo, S. García-Garabal, L. Segade, C. Franjo, O. Cabeza, *Fluid Phase Equilib.* **2009**, *278*, 36 – 40.
[32] G. Wedler, H.-J. Freund, *Physikalische Chemie*, Wiley-VCH, Weinheim, **2012**, p. 2.
[33] K. Scheffler, J. Straub, *Wasserdampftafeln*, Springer, Berlin, **1981**, p. 67, 64 Taf.
[34] M. Conde, *Int. J. Therm. Sci.* **2004**, *43*, 367 – 382..
[35] L. A. Leites, G. I. Magdanurov, S. S. Bukalov, R. West, *Mendeleev Commun.* **2008**, *18*, 14 – 15.
[36] L. Glasser, H. D. B. Jenkins, *Inorg. Chem.* **2008**, *47*, 6195 – 6202.
[37] F. L. Hirshfeld, *Theor. Chim. Acta* **1977**, *44*, 129 – 138.
[38] a) J. J. McKinnon, M. A. Spackman, A. S. Mitchell, *Acta Crystallogr. Sect. B* **2004**, *60*, 627 – 668; b) S. K. Wolff, D. J. Grimwood, J. J. McKinnon, M. J. Turner, D. Jayatilaka, M. A. Spackman, *CrystalExplorer (Version 3.1)*, University of Western Australia, **2012**.
[39] W. Beichel, U. P. Preiss, B. Benkmil, G. Steinfeld, P. Eiden, A. Kraft, I. Krossing, *Z. Anorg. Allg. Chem.* **2013**, *639*, 2153 – 2161.
[40] H. K. Stassen, R. Ludwig, A. Wulf, J. Dupont, *Chem. Eur. J.* **2015**, *21*, 8324 – 8335.
[41] G. M. Sheldrick, *Acta Crystallogr. Sect. A* **2008**, *64*, 112 – 122.
[42] a) L. J. Farrugia, *J. Appl. Crystallogr.* **1999**, *32*, 837 – 838; b) M. Nardelli, *J. Appl. Crystallogr.* **1995**, *28*, 659; c) C. F. Macrae, P. R. Edgington, P. McCabe, E. Pidkock, G. P. Shields, R. Taylor, M. Towler, J. van der Streek, *J. Appl. Crystallogr.* **2006**, *39*, 453 – 457.
[43] A. K. Burrell, R. E. D. Sesto, S. N. Baker, T. M. McCleskey, G. A. Baker, *Green Chem.* **2007**, *9*, 449 – 454.
[44] L. Han, H. Li, S.-J. Choi, M.-S. Park, S.-M. Lee, Y.-J. Kim, D.-W. Park, *Appl. Catal. A* **2012**, *429 – 430*, 67 – 72.
[45] J. Li, Y. Peng, G. Song, *Catal. Lett.* **2005**, *102*, 159 – 162.

Received: June 8, 2016
Published online on September 20, 2016

Please note: Minor changes have been made to this manuscript since its publication in *Chemistry–A European Journal* Early View. The Editor.

